Entropy **2015**, *17*, 5218-5240; doi:10.3390/e17085218

OPEN ACCESS
entropy
ISSN 1099-4300
www.mdpi.com/journal/entropy

Article

An Integrated Index for the Identification of Focal Electroencephalogram Signals Using Discrete Wavelet Transform and Entropy Measures

Rajeev Sharma [1], Ram Bilas Pachori [1,*] and U. Rajendra Acharya [2]

[1] Discipline of Electrical Engineering, Indian Institute of Technology Indore, Indore 452017, India; E-Mail: phd1301102007@iiti.ac.in

[2] Department of Electronics and Computer Engineering, Ngee Ann Polytechnic, Singapore 599489, Singapore; E-Mail: aru@np.edu.sg

* Author to whom correspondence should be addressed; E-Mail: pachori@iiti.ac.in; Tel.: +91-732-4240-716; Fax: +91-731-2361-482.

Academic Editor: Raúl Alcaraz Martínez

Received: 19 May 2015 / Accepted: 20 July 2015 / Published: 27 July 2015

Abstract: The dynamics of brain area influenced by focal epilepsy can be studied using focal and non-focal electroencephalogram (EEG) signals. This paper presents a new method to detect focal and non-focal EEG signals based on an integrated index, termed the focal and non-focal index (FNFI), developed using discrete wavelet transform (DWT) and entropy features. The DWT decomposes the EEG signals up to six levels, and various entropy measures are computed from approximate and detail coefficients of sub-band signals. The computed entropy measures are average wavelet, permutation, fuzzy and phase entropies. The proposed FNFI developed using permutation, fuzzy and Shannon wavelet entropies is able to clearly discriminate focal and non-focal EEG signals using a single number. Furthermore, these entropy measures are ranked using different techniques, namely the Bhattacharyya space algorithm, Student's t-test, the Wilcoxon test, the receiver operating characteristic (ROC) and entropy. These ranked features are fed to various classifiers, namely k-nearest neighbour (KNN), probabilistic neural network (PNN), fuzzy classifier and least squares support vector machine (LS-SVM), for automated classification of focal and non-focal EEG signals using the minimum number of features. The identification of the focal EEG signals can be helpful to locate the epileptogenic focus.

Keywords: EEG; epilepsy; wavelet; entropy; classifier

1. Introduction

Epilepsy is characterized by seizures, which may be due to epileptogenesis [1,2]. Epilepsy affects the quality of the patient's life and may lead to social impairment [3]. Patients of generalized and partial epilepsy can develop resistance to drugs during the course of epilepsy. The proportion of such patients is approximated to be 20% in generalized epilepsy and 60% in partial epilepsy [3]. In order to treat such patients surgically, the brain area involved in epileptic seizure generation needs to be removed. In this way, the identification of the brain area participating in seizure generation becomes an important step before the surgery.

Various techniques are developed to understand the dynamics of epileptogenic focus based on electroencephalogram (EEG) signals. These techniques can be useful to identify the epileptogenic focus. In the literature, to study the characteristics of epileptogenic focus, many non-linear parameters, like linear correlation, mutual information and phase synchronization with surrogate analysis [4], the time-variant connectivity measure and modified effective connectivity measure [5], coherence patterns [6], mean phase coherence establishing inter-electrode synchrony [7], moving window correlation dimension [8], *etc*., are examined. Results presented in these studies show that non-linear parameters are significantly useful for epileptogenic focus localization. The non-linear parameters extracted from EEG signals can be helpful to represent the non-linear dynamics of the brain [2].

Recently, Andrzejak *et al.* analyzed the bivariate EEG signals recorded intracranially from the patients of partial epilepsy [9]. The recordings from the epileptogenic focus are categorized as focal EEG signals, and recordings from other areas of the brain are defined as non-focal EEG signals. The identification of focal EEG signals can be used to locate the epileptogenic focus. Hence, the focal EEG signal classification is an important research problem. Epileptic activities in EEG signals are classified by extracting features from time, frequency, time-frequency and non-linear analysis of EEG signals [10]. The EEG signals are analyzed using wavelet transform and statistical pattern recognition in order to detect epileptic seizures [11]. In [12], discrete wavelet transform (DWT) is used for decomposition and classification of normal and epileptic EEG signals. Hence, features extracted from the time-frequency domain using DWT can be used to extract useful information from EEG signals. Entropy is a measure of variability within a signal [13]. It is a numerical descriptor that measures the randomness of a signal [14] and can be used to detect epilepsy using EEG signals [13,14].

In the present work, the automatic classification of the focal EEG signals is performed using DWT. The experimental results are presented for DWT from two to six levels. The proposed system used to perform the classification of focal and non-focal EEG signals is shown in Figure 1. Entropy measures, namely average Shannon wavelet entropy, average Rényi wavelet entropy and average Tsallis wavelet entropy, are computed from the energies of detail and approximate coefficients. The average fuzzy entropy, average permutation entropy and average phase entropies are computed from the sub-band signal reconstructed from the approximate coefficients. These computed entropy measures serve as the input feature set for different classifiers. Feature ranking methods, such as the Bhattacharyya space

algorithm, Student's t-test, the Wilcoxon test, the receiver operating characteristic (ROC) and entropy, are used to rank the features. These ranked features are used as the features for the classifiers, namely probabilistic neural network (PNN), k-nearest neighbour (KNN), fuzzy and least squares support vector machine (LS-SVM) for the classification of focal and non-focal EEG signals. We have also proposed a focal and non-focal index (FNFI) to discriminate focal and non-focal EEG signals.

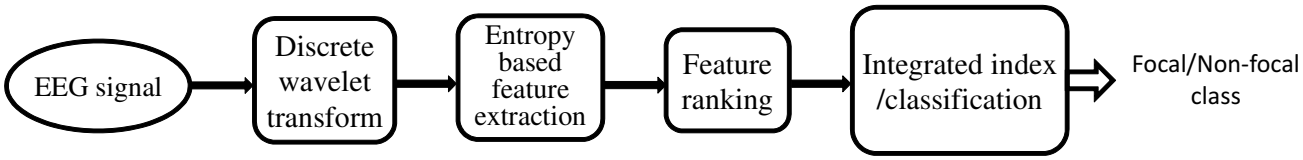

Figure 1. Block diagram of the proposed automatic classification system.

The remaining sections are arranged as follows: Section 2 describes the dataset used, the feature extraction, the ranking methods, classification and the integrated discrimination index. In Section 3, the results of this study are presented, and the results are discussed in Section 4. The paper concludes in Section 5.

2. Methodology

2.1. Dataset

The EEG recordings of focal and non-focal classes studied in this paper are taken from Bern Barcelona database (www.dtic.upf.edu/~ralph/sc/). Details of the database can be found in [9]. The database consists of bivariate EEG signals recorded intracranially from five patients of pharmacoresistant temporal lobe epilepsy. The time series in bivariate EEG signals are represented by "x" and "y". Each EEG signal has $10,240$ samples, sampled at a 512-Hz sampling frequency. The database consists of 3750 focal EEG signal pairs and 3750 non-focal EEG signal pairs. In this study, we have used 50 focal EEG signal pairs and 50 non-focal EEG signal pairs. The "x" time series of a focal EEG signal pair and a non-focal EEG signal pair are shown in Figure 2. Figure 3 depicts the "y" time series of focal EEG signal pair and non-focal EEG signal pair.

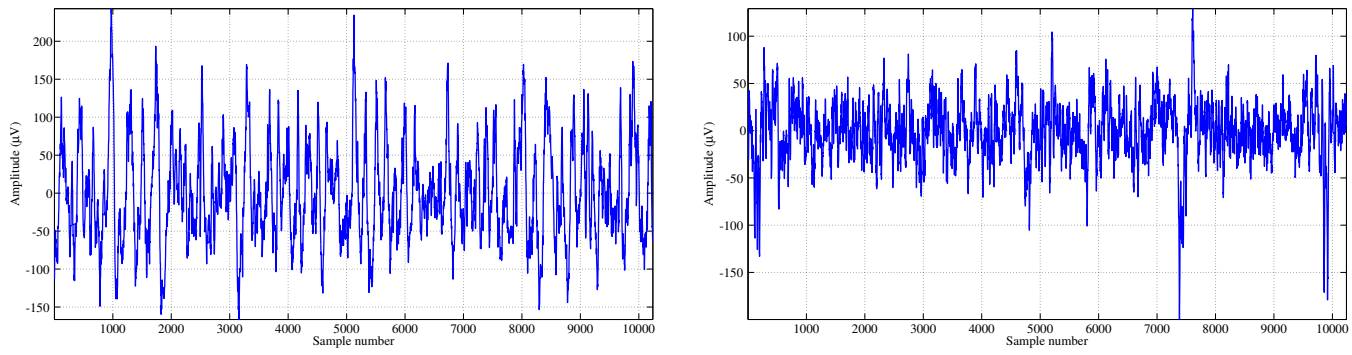

(a) (b)

Figure 2. Plot of the "x" time series of EEG signal pairs: (**a**) focal EEG signal; (**b**) non-focal EEG signal.

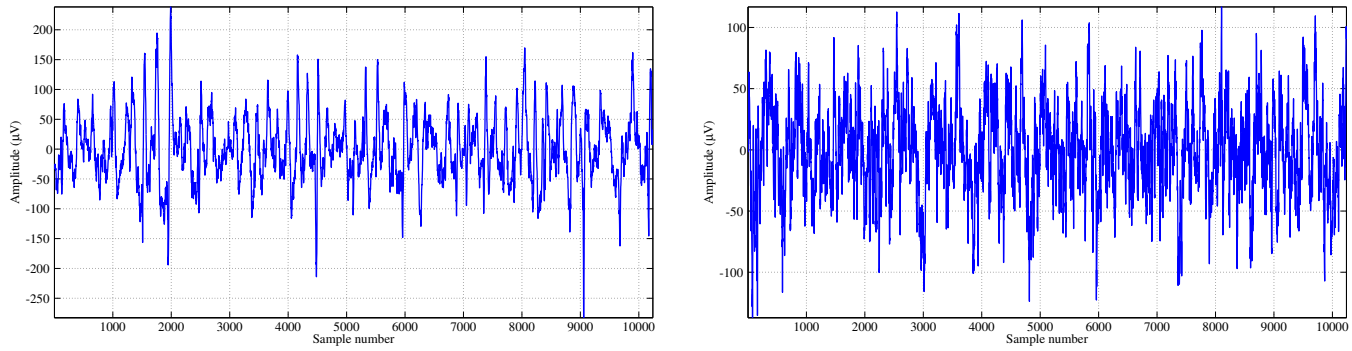

(a) (b)

Figure 3. Plot of the "y" time series of EEG signal pairs: (**a**) focal EEG signal; (**b**) non-focal EEG signal.

2.2. Feature Extraction

In order to perform the classification of focal and non-focal EEG signals, the extraction of features is an important step. Features are extracted from DWT coefficients of both "x" and "y" time series of EEG signal pairs. A brief description of DWT and entropy features is given in the following sections.

2.2.1. Discrete Wavelet Transform

The EEG signal is converted to the wavelet domain by performing discrete wavelet transform (DWT) [15]. In the DWT, the EEG signals are passed through the low pass filter (LPF) and high pass filter (HPF). The filtered signals are down-sampled by a factor of 2. This process converts the signals to low pass (approximate) and high pass (detail) coefficients. This procedure forms the first level of decomposition of the EEG signal. For the next level of decomposition, the approximate coefficients are again passed through the HPF and LPF, and the same process is repeated to obtain the next level of DWT coefficients. After each level of decomposition, the bandwidth obtained is half of the bandwidth of the previous level [16]. In this paper, the DWT of the EEG signals is performed up to six levels using Daubechies wavelet of order 4 (db4) [12], and then, Shannon, Rényi, Tsallis, permutation, phase and fuzzy entropies are extracted using these DWT coefficients.

2.2.2. Average Shannon Wavelet Entropy

In the Shannon wavelet entropy computation, the wavelet decomposition and Shannon entropy are incorporated together. This entropy measure provides the variability associated with different frequency bands. The wavelet coefficients obtained by applying DWT are used to compute the energy of these detail and approximate sub-band signals. If E_i denotes the energy of the i-th sub-band signal computed from the wavelet coefficients, then the total signal energy can be given by [17]:

$$E_t = \sum_{i=1}^{K} E_i \tag{1}$$

where K denotes the total number of sub-band signals obtained from the DWT of the EEG signal. The relative wavelet energy can be defined as [17]:

$$q_i = \frac{E_i}{E_t} \tag{2}$$

Finally, wavelet entropy using Shannon entropy formula can be defined as [17]:

$$Swn = -\sum_{i=1}^{K} q_i \log(q_i) \tag{3}$$

If Swn_x and Swn_y denote the Swn of the "x" and "y" time series of EEG signal, respectively, then the average Shannon wavelet entropy of the signal can be defined as:

$$Swn_{Avg} = \frac{Swn_x + Swn_y}{2} \tag{4}$$

2.2.3. Average Rényi Wavelet Entropy

We have used the formula proposed by Rényi [18] to compute the wavelet entropy of EEG signal from q_i. The Rényi wavelet entropy can be defined as [18]:

$$Rwn_\alpha = \frac{1}{1-\alpha} \log \left(\sum_{i=1}^{K} q_i^\alpha \right), \quad \alpha \neq 1 \tag{5}$$

In this paper, the value of α is taken as 2. For $\alpha = 2$, Rényi entropy is also called Rényi's quadratic entropy and can be given as [13]:

$$Rwn_2 = -\log \left(\sum_{i=1}^{K} q_i^2 \right) \tag{6}$$

The average Rényi wavelet entropy in terms of the Rényi wavelet entropies of the "x" (Rwn_x) and "y" (Rwn_y) time series of EEG signal can be defined as:

$$Rwn_{Avg} = \frac{Rwn_x + Rwn_y}{2} \tag{7}$$

2.2.4. Average Tsallis Wavelet Entropy

Tsallis wavelet entropy is presented in [19], which uses the Tsallis entropy formula to compute entropy from q_i of the signal. In [19], it is shown that the Tsallis wavelet entropy can extract improved features by reducing the negative effects of wavelet aliasing. In [19], Tsallis entropy is computed using the sliding window for a signal. In this paper, we have used the Tsallis entropy formula to compute the Tsallis wavelet entropy without using any window. The Tsallis wavelet entropy can be defined as [19,20]:

$$Twn_a = \frac{1}{a-1} \left(1 - \sum_{i=1}^{K} q_i^a \right), \quad a \neq 1 \tag{8}$$

where parameter a is called the nonextensivity index [19]. In this work, $a = 2$ is considered for Tsallis wavelet entropy computation. The average Tsallis wavelet entropy can be computed as:

$$Twn_{Avg} = \frac{Twn_x + Twn_y}{2} \tag{9}$$

where Twn_x and Twn_y are the Tsallis wavelet entropy obtained for the "x" time series and the "y" time series of the pair of EEG signal, respectively.

2.2.5. Average Fuzzy Entropy

Fuzzy entropy is developed based on the concept of fuzzy sets. In [21], the authors applied the fuzzy entropy measure on the surface electromyogram (EMG) signal by employing the family of exponential functions as a fuzzy membership function [22]. In this paper, we have computed the fuzzy entropy of EEG signals, based on the approach presented in [21]. The fourth level approximate component obtained from the DWT of the EEG signal is used for the computation of fuzzy entropy. In the computation of fuzzy entropy, three parameters need to be determined. The first parameter is the length of sequence to be compared, denoted by m, and the other two parameters are r and n. The width of the boundary of the exponential function is controlled using parameter r, and parameter n determines the gradient of the boundary of exponential function. In this work, to compute the fuzzy entropy of the approximate component of the wavelet transform of EEG signals, the values of $r = 0.2$ and $n = 2$ are fixed [21], and for $m = 2, 3, 4$, fuzzy entropies are computed. We have considered $m = 4$ for our experiment, because the p-value obtained for the discrimination of focal and non-focal classes with $m = 4$, $p = 4.04 \times 10^{-7}$ is better than $p = 2.17 \times 10^{-6}$ for $m = 3$. The p-value for $m = 2$ is 8.72×10^{-6}; thus, the $m = 4$ is a suitable choice for fuzzy entropy computation. Finally, the average of the fuzzy entropy ($Fzen_{Avg}$) is computed for the "x" and "y" time series of pair of EEG signal.

2.2.6. Average Permutation Entropy

In permutation entropy, the variation of predefined symbols in the neighboring samples is quantified [23]. The computation of the permutation entropy requires the determination of embedded dimension m and time lag τ. The total number of possible symbols depends on the value of m. For a given value of m, a total of $m!$ permutations are possible. Each permutation can be considered as a symbol. Based on the parameters m and τ from a time series, the embedded time vector is formed. In the time series vector, the probability distribution of the each symbol is computed. If t_k represents the number of occurrences of the k-th symbol in the time series, then the probability of occurrence of the k-th permutation can be estimated as [24]:

$$s_k = \frac{t_k}{N - m + 1} \tag{10}$$

where N is length of the signal. The permutation entropy in terms of s_k can be given as [23]:

$$Pen = -\sum_{k=1}^{K} s_k \log(s_k) \tag{11}$$

where K is the number of symbols for a given embedded dimension. A smaller value of the Pen indicates more regularity present in the time series [23]. In [24], the value of m suggested is from 3 to 7. Various studies for the application of Pen on EEG signals are compared in [25], and it can be observed that the values $m = 3$ and $\tau = 1$ are commonly used. In this work, we have taken $m = 3$ and $\tau = 1$ for the computation of Pen. If Pen_x and Pen_y represent the permutation entropy of the "x" time series and the "y" time series of the pair of EEG signal, then the average permutation entropy can be given as:

$$Pen_{Avg} = \frac{Pen_x + Pen_y}{2} \tag{12}$$

2.2.7. Average Phase Entropies

The spectral representation of higher order moments, like third order moments, is known as higher order spectra (HOS) [14]. The computation of the phase entropies employs the bispectrum, which is the spectrum of third order moments. The bispectrum of a signal can be represented by $\beta(F_1, F_2)$, which is a function of two frequency components F_1 and F_2, and can be defined as [26]:

$$\beta(F_1, F_2) = E[X(F_1)X(F_2)X^*(F_1 + F_2)] \tag{13}$$

where $X(F)$ represents the Fourier transform of a signal and X^* denotes the complex conjugate. The two probabilities can be estimated in terms of the L^1 and L^2 norms of the bispectrum as [27]:

$$u_k = \frac{|\beta(F_1, F_2)|}{\sum_{\xi} |\beta(F_1, F_2)|} \tag{14}$$

$$v_j = \frac{|\beta(F_1, F_2)|^2}{\sum_{\xi} |\beta(F_1, F_2)|^2} \tag{15}$$

where ξ represents the non-redundant region [14]. The phase entropies $Hen1$ and $Hen2$ can be defined in terms of these probability estimates u_k and v_j as [14,27]:

$$Hen1 = -\sum_{k} u_k \log(u_k) \tag{16}$$

and:

$$Hen2 = -\sum_{j} v_j \log(v_j) \tag{17}$$

The phase entropies are utilized as features for the diagnosis of epileptic EEG signals automatically in [14]. In this paper, average phase entropies $Hen1_{Avg}$ and $Hen2_{Avg}$ computed from the fourth level approximate component obtained from DWT of EEG signal are defined as [28]:

$$Hen1_{Avg} = \frac{Hen1_x + Hen1_y}{2} \tag{18}$$

and:

$$Hen2_{Avg} = \frac{Hen2_x + Hen2_y}{2} \tag{19}$$

where $Hen1_x$ and $Hen2_x$ represent the notations of $Hen1$ and $Hen2$ of the "x" time series of EEG signals, respectively. The entropies $Hen1_y$ and $Hen2_y$ are $Hen1$ and $Hen2$ of the "y" time series of EEG signals.

2.3. Feature Ranking

The feature ranking step helps to select the most relevant features from the available features. Based on ranking, the features with higher ranks can be selected, and features with lower rank can be ignored [29]. Thus, the minimum number of features required to obtain the highest classification accuracy can be obtained using feature ranking methods. This reduces the complexity of the classifier without sacrificing its performance [16]. In this work, Bhattacharyya space algorithm, Student's t-test, Wilcoxon method, receiver operating characteristic (ROC) method and entropy-based feature ranking methods are used for feature selection. A brief explanation of these methods is given as follows:

2.3.1. Bhattacharyya Space Algorithm

This method uses the Bhattacharyya distance, which is a measure of the separability between two populations [29,30]. The ranking of features is performed based on the discrimination ability of features.

2.3.2. Student's t-Test

The Student's t-test evaluates the population mean and uses it to determine the discrimination between two groups [16]. As a result of this test, the t-value is obtained for the computed feature of two classes. In order to rank the features, the t-value is used. The features with a higher t-value are considered to have more discriminative ability [31].

2.3.3. Wilcoxon Test

The Wilcoxon test belongs to the class of nonparametric tests, which uses a rank-based procedure [32]. In this method, the two-sample unpaired Wilcoxon test is applied for feature ranking [33]. The method is also referred as the Wilcoxon–Mann–Whitney test and employs the magnitude of resultant U-statistics to rank the features [34,35].

2.3.4. Entropy

In the entropy method for feature reduction, the divergence is used to measure distance between the probability density functions, which is a form of Kullback–Leibler distance [36]. The features with higher divergence are considered more suitable for discriminating classes.

2.3.5. Receiver Operating Characteristic Method

In this method, the receiver operating characteristic (ROC) is drawn between sensitivity and 1-specificity, for different values of the threshold. Based on the area under the ROC curve, ranking of the features is performed [29,36].

2.4. Classification

In this work, classification of focal EEG signals is performed using different classifiers. The goal is to find out the maximum classification accuracy. A ten-fold cross-validation procedure is followed for testing the performance of classifiers [37]. In this procedure, the available dataset is divided into ten random sets of equal size. Nine sets are used to train the classifier, and the remaining set is utilized for the evaluation of classifier performance. The whole process is repeated ten times, without repeating any set for classification. Finally, the performance evaluation parameters are computed by taking the average of all ten folds. The classifiers used in this work are briefly explained as follows.

2.4.1. Probabilistic Neural Network

The probabilistic neural network (PNN) classifier employs a four-layer architecture for classification [38]. The PNN classifier consists of feed forward networks of neurons arranged in layers.

The input layer is the first layer, which simply passes the input to the pattern layer neurons [39]. The obtained output from the pattern layer is summed up and averaged at the summation layer. The summation layer also estimates the maximum likelihood of a pattern being classified. Finally, the decision of the class is made at the decision layer based on Bayes's decision rule [39]. The selection of smoothing parameter [39] denoted by σ_1 is required for performing classification using PNN classifier.

2.4.2. k-Nearest Neighbour

In k-nearest neighbour (KNN) classifier, an unknown sample is classified using the relation of the unknown sample with the known nearest samples [38]. The closeness of the k-nearest sample is determined using distance or similarity criteria [40]. It is considered that the near samples have more contribution than the far samples. Finally, the unknown sample is considered to belong to the class that is common among the k-nearest neighbors.

2.4.3. Fuzzy Sugeno Classifier

In the fuzzy classification, instead of considering that the sample belongs to a particular class, the sample is considered to be a member of each class with a different membership function. The class of the sample is determined based on fuzzy if-then rules [41]. In the fuzzy Sugeno classifier, the fuzzy inference system (FIS) is generated using the subtractive clustering technique [42]. The behavior of the fuzzy system is determined by FIS. Clusters in the FIS are fixed by the radius (R). The input and output membership functions of the classifier used in this paper are Gaussian and linear, respectively [43].

2.4.4. Least Squares Support Vector Machine

The support vector machine (SVM) [44] classifier can be used for both linear and non-linear classification, by selecting the suitable kernels [23]. The SVM method performs the mapping of the data into higher dimensional space, where it can be separated using a decision boundary. In order to find the decision boundary, the margin between two hyperplanes associated with support vectors of two different classes is maximized [23]. The problem of finding a decision boundary can be formulated as an optimization problem subjected to inequality constraints [45]. The least squares support vector machine (LS-SVM) provides the least squares solution of the optimization problem [45]. The classification of EEG signals of different classes has been studied using SVM classifier and LS-SVM classifier in [28,46–48]. The radial basis function (RBF) [28] is used as a kernel in this work to form the decision boundary. The width of the RBF kernel function can be controlled using a parameter [47] denoted by σ_2.

2.5. Integrated Discrimination Index

The significant features can be used to derive an expression, such that for each class, the expression results in a unique range of values [49–54]. Such an index can be used to characterize the state of a physiological condition [49]. Using a single index, two or more classes can be discriminated. This concept of the integrated index is used to diagnose diabetes using heart rate signals [50], coronary artery

disease (CAD) using ultrasound images [51], malignant and benign thyroid using ultrasound images [52], CAD using heart rate signals [53] and diabetes retinopathy using fundus images [54].

In this work, significant features are used to derive an integrated discrimination index, namely the focal and non-focal index (FNFI). The significant features are selected based on the class discrimination ability and the classification performance of the features. Based on trial and error experiments, FNFI can be given as:

$$\text{FNFI} = 10 \times \left[\alpha_1(n_1 + \frac{1}{\beta_1}n_2) - n_3\frac{1}{\gamma_1}\right] \tag{20}$$

where n_1, n_2 and n_3 are the values of the three features extracted from focal and non-focal EEG signals. The coefficients α_1, β_1 and γ_1 are optimized in order to obtain a unique range of FNFI for each class. The coefficients of the formula in (20) are determined using the genetic algorithm (GA). GA is an optimization algorithm based on the law of natural selection and genetics [55]. It is less sensitive to initial conditions. It successively searches the optimal solution of a problem using selection, crossover and mutation operations [56].

3. Results

In this work, we have extracted seven entropy features from the DWT of focal and non-focal EEG signals. Using these extracted features, the classification of the EEG signals corresponding to focal and non-focal classes is performed. The performance of the four classifiers is presented for the second to sixth levels of DWT decomposition. The highest classification performance is found at the fourth level of DWT.

The sub-band signals obtained from the fourth level of DWT coefficients are shown in Figure 4. Figure 4a shows the focal EEG signal and its four detail (d1-d4) and approximate (a4) sub-band signals. Similarly, four detail and approximate sub-band signals of the non-focal EEG signal are shown in Figure 4b. The entropies Swn_{Avg}, Rwn_{Avg} and Twn_{Avg} are computed using energies of d1–d4 and a4 sub-band signals. The other entropies, $Fzen_{Avg}$, $Hen1_{Avg}$, $Hen2_{Avg}$ and Pen_{Avg}, are computed from a4 sub-band signal. Similarly, the features are computed from other levels of the DWT decomposition of the EEG signals.

Table 1. p-values obtained as a result of Kruskal–Wallis statistical test for feature discrimination at different DWT levels.

Feature	Wavelet decomposition level				
	2	3	4	5	6
Swn_{Avg}	6.000×10^{-4}	6.565×10^{-5}	9.182×10^{-7}	9.511×10^{-8}	1.901×10^{-6}
Rwn_{Avg}	2.332×10^{-6}	1.336×10^{-7}	1.901×10^{-6}	6.565×10^{-5}	7.000×10^{-4}
Twn_{Avg}	7.000×10^{-4}	8.760×10^{-5}	1.495×10^{-6}	1.026×10^{-7}	2.761×10^{-6}
$Fzen_{Avg}$	6.722×10^{-9}	5.701×10^{-9}	4.042×10^{-7}	5.766×10^{-1}	2.495×10^{-6}
$Hen1_{Avg}$	4.710×10^{-2}	2.890×10^{-2}	6.300×10^{-3}	2.510×10^{-2}	4.906×10^{-1}
$Hen2_{Avg}$	2.090×10^{-2}	1.770×10^{-2}	1.160×10^{-2}	2.990×10^{-2}	3.379×10^{-1}
Pen_{Avg}	2.690×10^{-2}	1.092×10^{-5}	$\mathbf{5.253 \times 10^{-10}}$	5.729×10^{-6}	1.638×10^{-1}

The Kruskal–Wallis statistical test [57] has been applied for determining the discrimination ability of features extracted from epileptic seizure EEG signals [58–60] and RR-interval (interval between adjacent QRS complexes of electrocardiogram) signals [61]. In order to examine the class discrimination ability of the features, the Kruskal–Wallis statistical test is applied on all features, and the resultant p-values are shown in Table 1. The box plots of various entropy features computed for the second to sixth levels of the DWT-based decomposition are presented in Figures 5–9. The lowest p-value of a feature is indicated by bold entry in Table 1. It can be noticed from Table 1 that Pen_{Avg} obtained from the fourth level approximate sub-band signal has the lowest p-value, indicating the highest discrimination ability among all features.

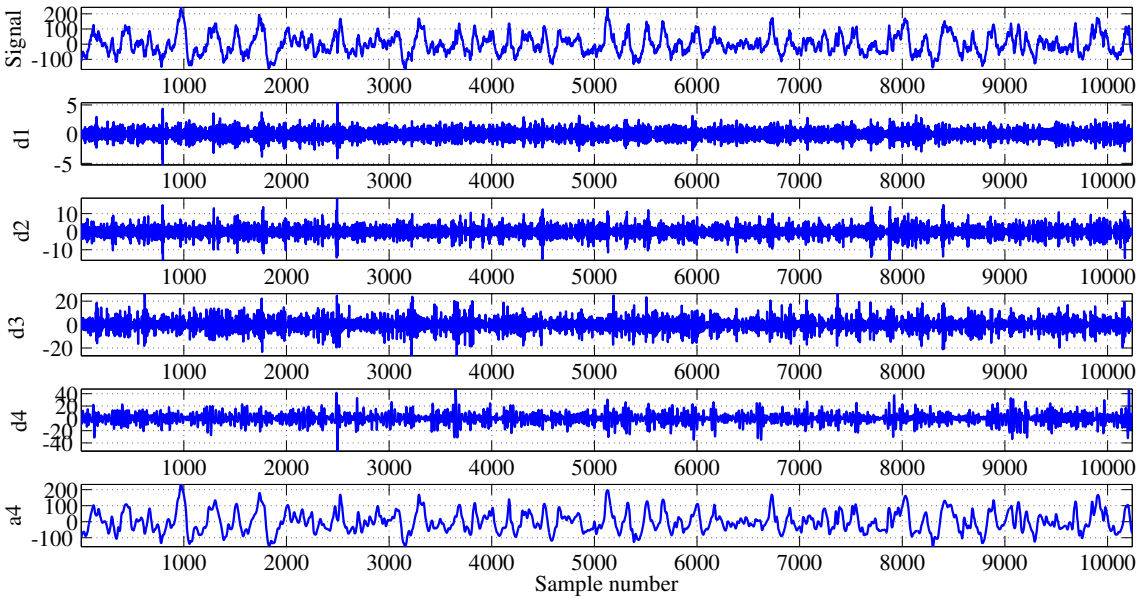

(a)

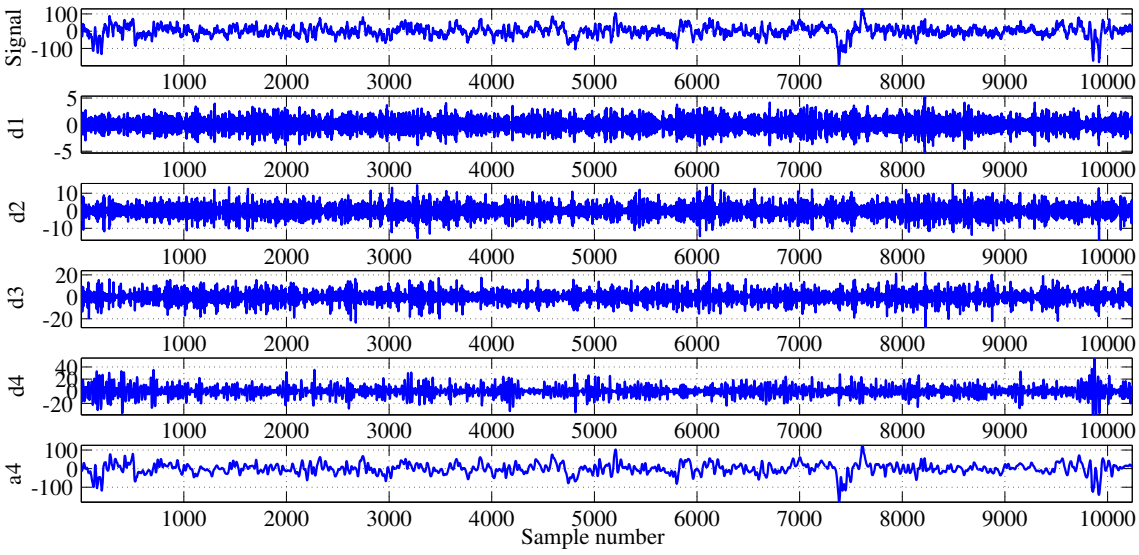

(b)

Figure 4. EEG signal and its decomposition using DWT: (**a**) focal and (**b**) non-focal.

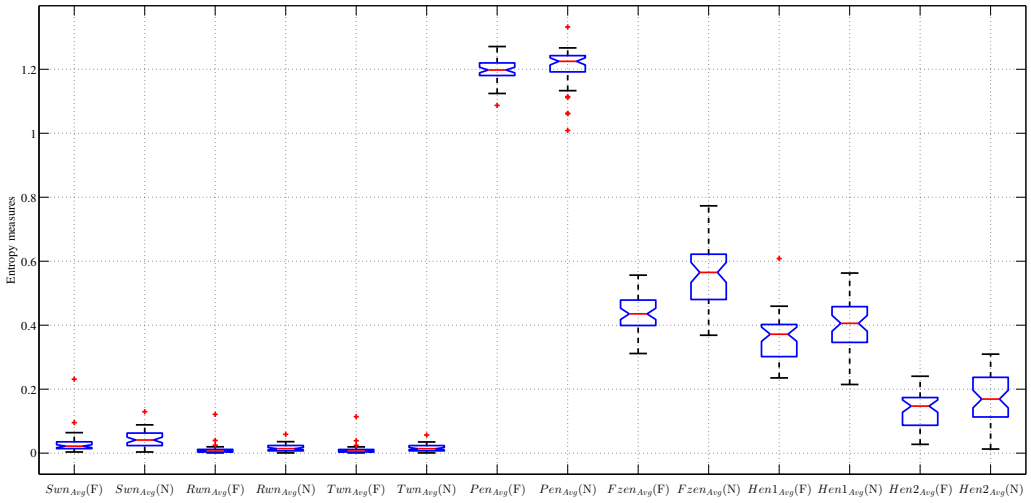

Figure 5. Boxplots of various entropies computed from the second level of DWT for focal (F) and non-focal (N) EEG signals.

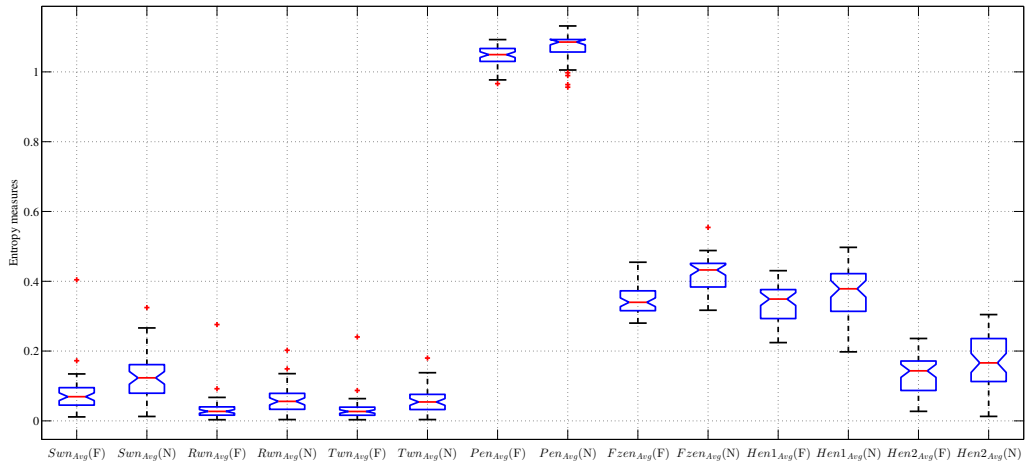

Figure 6. Boxplots of various entropies computed from the third level of DWT for focal (F) and non-focal (N) EEG signals.

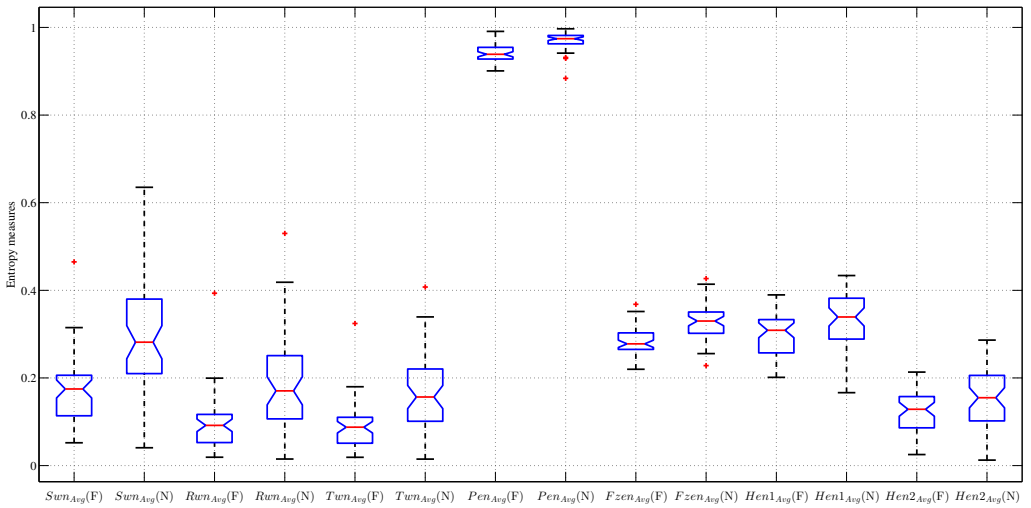

Figure 7. Boxplots of various entropies computed from the fourth level of DWT for focal (F) and non-focal (N) EEG signals.

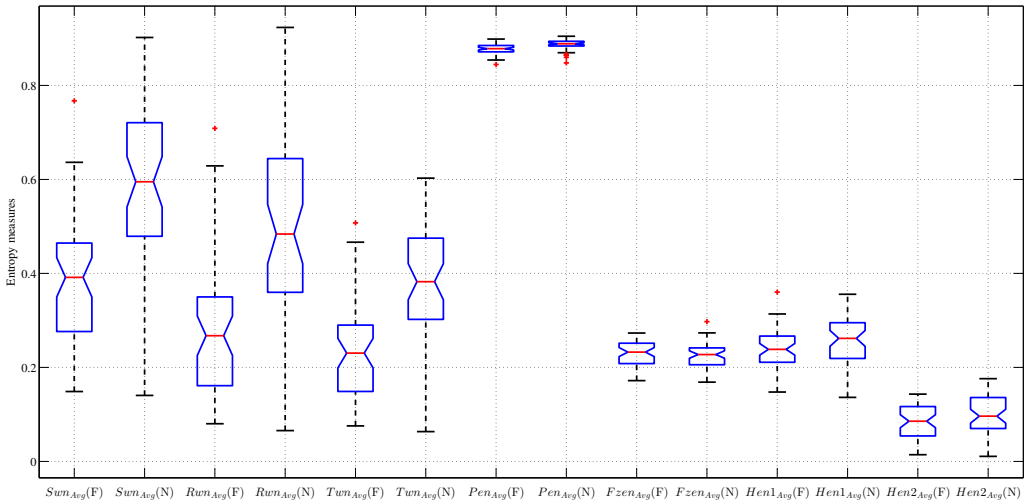

Figure 8. Boxplots of various entropies computed from the fifth level of DWT for focal (F) and non-focal (N) EEG signals.

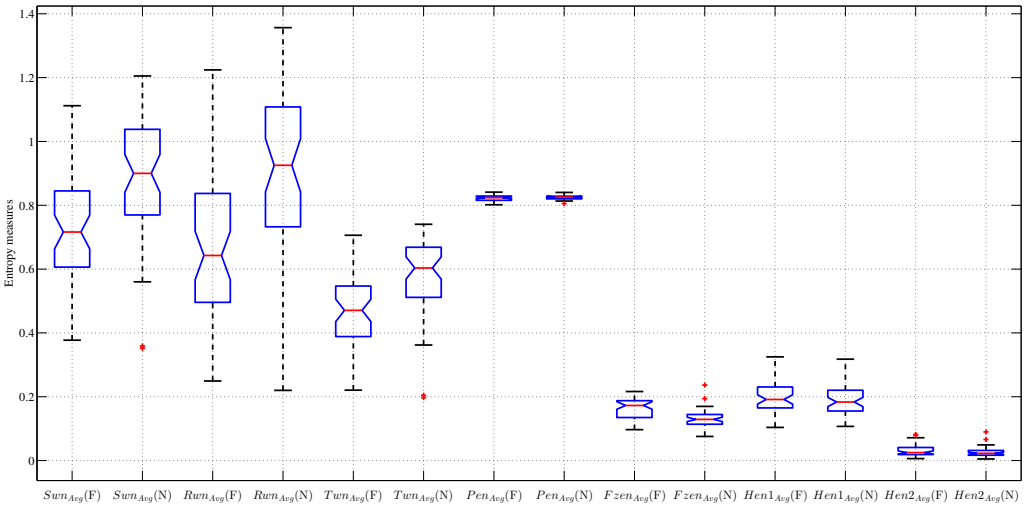

Figure 9. Boxplots of various entropies computed from the sixth level of DWT for focal (F) and non-focal (N) EEG signals.

The range of features computed from the fourth level of DWT is presented in Table 2. Before performing the classification, features are ranked using different feature ranking methods. The classification accuracies of various classifiers are shown in Table 3. The parameters of the classifiers are selected on the basis of trial and error experiments. The parameters corresponding to the maximum classification accuracy are mentioned in Table 3. In this work, the classification accuracy for classification of focal EEG signals is computed using ten-fold cross-validation procedure. The obtained highest classification accuracies are shown by bold entries in Table 3. It can be observed from Table 3 that the LS-SVM classifier with features obtained from the fourth level of DWT-based decomposition results in the highest classification accuracy. Hence, we formulated FNFI using the features extracted from the fourth level of DWT-based decomposition. The plot of the classification accuracy obtained using the LS-SVM classifier *versus* the number of features used for different feature ranking methods is shown in Figure 10. The ranking of features, using Student's t-test, is as Pen_{Avg}, $Fzen_{Avg}$, Swn_{Avg},

Twn_{Avg}, Rwn_{Avg}, $Hen1_{Avg}$ and $Hen2_{Avg}$. Except for the last two features, all (first five) features were ranked in the same order for Student's t-test and ROC methods. Therefore, the plots corresponding to Student's t-test and ROC overlap each other in Figure 10. The highest performance using the minimum number of features for various ranking methods using the LS-SVM classifier is presented in Table 4. It can be noticed from Table 4 that the LS-SVM classifier with only the first three ranked features using the Student's t-test and ROC methods provided the highest performance. These three features are Pen_{Avg}, $Fzen_{Avg}$ and Swn_{Avg}. The performance of the classifier is measured in terms of accuracy (Acc), sensitivity (Sen) and specificity (Spe) [62]. The highest values of Acc, Sen, and Spe obtained are 84%, 84% and 84%, respectively, using the ten-fold cross-validation method for focal and non-focal EEG signals classification. Table 4 shows the mean $\pm$ standard deviation of the obtained performance evaluation parameters (Acc, Sen, and Spe) during ten-folds cross-validation procedure using LS-SVM classifier for different ranking methods.

Table 2. Range distribution (mean $\pm$ standard deviation) of different entropy features extracted from the fourth level of DWT for focal and non-focal classes.

Feature	Focal EEG signals	Non-focal EEG signals	t-value
Swn_{Avg}	0.1764 ± 0.0782	0.2874 ± 0.1230	5.3831
Rwn_{Avg}	0.0970 ± 0.0617	0.1810 ± 0.1023	4.9688
Twn_{Avg}	0.0904 ± 0.0521	0.1606 ± 0.0813	5.1419
$Fzen_{Avg}$	0.2841 ± 0.0321	0.3254 ± 0.0400	5.6913
$Hen1_{Avg}$	0.3002 ± 0.0470	0.3304 ± 0.0628	2.7250
$Hen2_{Avg}$	0.1212 ± 0.0499	0.1536 ± 0.0676	2.7228
Pen_{Avg}	0.9414 ± 0.0205	0.9698 ± 0.0196	7.0752

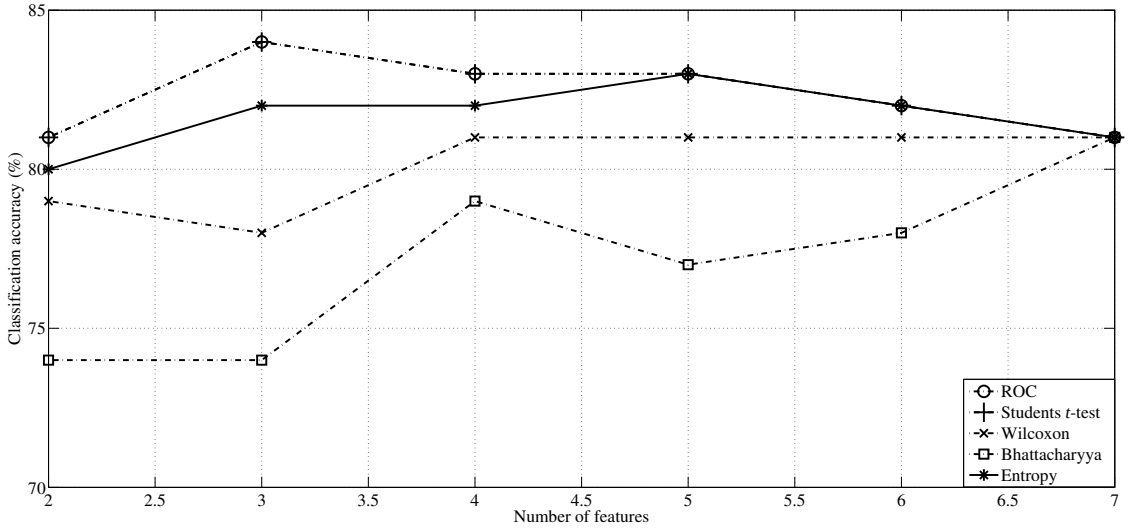

Figure 10. Plot of average classification accuracy (obtained using the LS-SVM classifier) *versus* the number of features for various feature ranking methods.

Table 3. Classification accuracy (%) obtained using different classifiers for features extracted from various sub-bands of DWT. PNN, probabilistic neural network; KNN, k-nearest neighbour; LS-SVM, least squares support vector machine.

DWT based decomposition level	Classifier	ROC	Student's t-test	Bhatacharyya space algorithm	Entropy	Wilcoxon
Second	KNN ($k = 1$)	72	75	75	75	75
	PNN ($\sigma_1 = 0.41$)	79	81	80	80	80
	Fuzzy ($R = 0.1$)	80	79	81	81	81
	LS-SVM ($\sigma_2 = 3.6$)	77	79	81	82	81
Third	KNN ($k = 1$)	75	75	70	70	70
	PNN ($\sigma_1 = 0.21$)	79	78	79	79	79
	Fuzzy ($R = 0.1$)	81	81	80	81	80
	LS-SVM ($\sigma_2 = 4.2$)	81	80	79	78	80
Fourth	KNN ($k = 1$)	70	70	74	68	72
	PNN ($\sigma_1 = 0.31$)	80	80	78	75	76
	Fuzzy ($R = 0.1$)	82	82	81	82	79
	LS-SVM ($\sigma_2 = 4.2$)	**84**	**84**	81	83	81
Fifth	KNN ($k = 1$)	61	61	63	68	68
	PNN ($\sigma_1 = 0.21$)	75	75	75	75	79
	Fuzzy ($R = 0.1$)	78	78	78	79	81
	LS-SVM ($\sigma_2 = 8.6$)	77	78	77	77	79
Sixth	KNN ($k = 1$)	70	67	70	67	71
	PNN ($\sigma_1 = 0.21$)	73	75	73	75	75
	Fuzzy ($R = 0.1$)	78	78	78	76	78
	LS-SVM ($\sigma_2 = 6.8$)	76	77	76	78	77

Table 4. Best performance of the proposed system using different ranking methods. Acc, accuracy; Sen, sensitivity; Spe, specificity.

Ranking method	Number of features	Acc (%)	Sen (%)	Spe (%)
Bhattacharyya space algorithm	7	81 ± 8.75	78 ± 14.75	84 ± 12.65
Student's t-test	3	84 ± 10.74	84 ± 15.77	84 ± 12.66
Wilcoxon	4	81 ± 12.86	80 ± 21.08	82 ± 19.88
ROC	3	84 ± 10.74	84 ± 15.77	84 ± 12.66
Entropy	5	83 ± 10.59	82 ± 14.75	84 ± 12.64

Table 2 shows the ranges of extracted entropy features for focal and non-focal classes of EEG signals and the corresponding t-values. It can be observed that Pen_{Avg}, $Fzen_{Avg}$ and Swn_{Avg} are more suitable for the discrimination of focal and non-focal EEG signals. These selected features are used to develop an FNFI for the discrimination of focal and non-focal classes. In (20), the values of the coefficients α_1, β_1 and γ_1 computed using GA are -1, -14 and -3, respectively. Figure 11 represents the distribution of the FNFI for focal and non-focal EEG signals. It can be observed in Figure 11 that FNFI results in the clear separation between two classes.

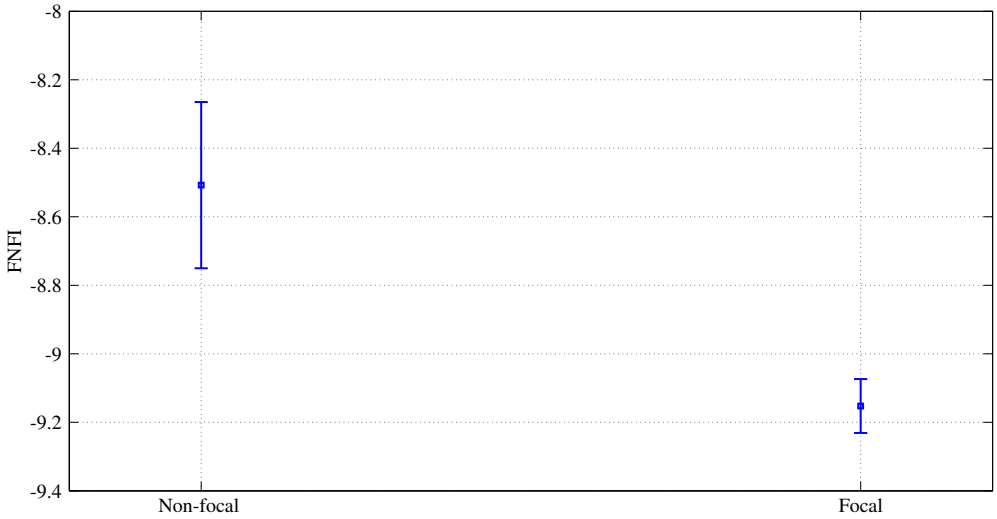

Figure 11. Distribution plot of FNFI for focal and non-focal EEG signals.

4. Discussion

The purpose of this study is to analyze the EEG signals acquired from the focal and non-focal area of epileptic brain by applying wavelet transform in order to localize the epileptogenic focus. Due to non-stationary nature of EEG signals, DWT is used to analyze focal and non-focal EEG signals. In order to determine the suitable DWT level, classification performance is evaluated using entropy features extracted from the second to sixth levels. We have obtained the highest classification performance using entropy features computed from the fourth-level DWT.

In [9], the randomness, non-linear independence and stationarity tests have been performed using surrogate analysis. This study has shown that EEG signals recorded from the epileptic brain area are more non-linear, less random and more stationary as compared to the EEG recordings from the nonepileptogenic brain area. Nonlinearity in focal and non-focal EEG signals has been studied using the non-linear prediction error and rank-based prediction score [63]. In this study, it is indicated that the degree of the non-linear deterministic structure is higher in focal EEG signals than non-focal EEG signals. Furthermore, non-focal EEG signals are found to be more non-stationary, as compared to focal EEG signals. In another study on the same database [64], univariate and bivariate recurrence network measures are applied to test the randomness and nonlinearity of focal and non-focal EEG signals. The average clustering coefficient, assortativity and average cross-clustering coefficients are found to be suitable to discriminate focal and non-focal EEG signals. This implies that focal EEG signals have a higher degree of structural complexity and interdependency as compared to non-focal EEG signals. Entropy is a non-linear parameter; hence, it can effectively capture the non-linear activities of the central nervous system and human brain [2,13,14]. The box plots depicted in Figures 5–9 show that the Swn_{Avg}, Rwn_{Avg} and Twn_{Avg} consistently have lower values for focal EEG signals as compared to non-focal EEG signals for all levels of DWT. It can also be observed that as the level of DWT-based decomposition increases, the entropy values of Swn_{Avg}, Rwn_{Avg} and Twn_{Avg} also increase. The Pen_{Avg}, $Fzen_{Avg}$, $Hen1_{Avg}$ and $Hen2_{Avg}$ also exhibit higher values for non-focal EEG signals as

compared to focal EEG signals from the second to fourth levels of DWT decomposition. The Pen_{Avg}, $Hen1_{Avg}$ and $Hen2_{Avg}$ show smaller values for focal EEG signals at the fifth level of DWT as compared to non-focal EEG signals. The observed trend of entropy features from the second to fourth level of DWT-based decomposition suggests that the values of entropy features for focal EEG signals are smaller than non-focal EEG signals. The entropy of a signal measures the complexity present in the signal [24]. A lower value of the entropy indicates the presence of less complexity and more regularity in the signal. In other words, focal EEG signals are more regular may be due to the synchronized electrical activities of neurons in the epileptogenic brain area.

In [65], the temporal dynamics of epileptogenic focus is studied using the frequency-entropy (FE) templates. In this method, the FE template of the inter-ictal recording is compared with the reference template in different electrodes, and it is suggested that the high template similarity can be used as an indicator of epileptogenic focus. In [66], the delta asymmetry is shown to be useful for epileptic focus determination in 83% of patients. In [67], an algorithm for focus localization is presented using improved transfer entropy measures. These information flow-based measures reliably identified the epileptogenic focus in four patients. The local field potential synchrony showed lower values in seizure-generating brain [68]. They concluded that the epileptic brain region is functionally isolated from other brain regions. In these methods, the epileptogenic zone is localized using different non-linear parameters on the recorded EEG signals. In the proposed method, we have classified the EEG signals recorded from the focal and other areas of brain, which can be used for epileptogenic focus localization. We have compared our proposed method with the existing automated methods, which used the same database (Table 5). In [69], two subsets of focal and non-focal EEG classes of sizes of 50 and 750 pairs of EEG signals are analyzed. Only the single-channel recordings of focal and non-focal EEG signals are used for classification. In order to classify focal and non-focal classes, the authors have used delay permutation entropy (DPE) and the SVM classifier. They obtained classification accuracy of 84% and 75% for the first 50 sets and 750 sets of EEG signals of focal and non-focal classes, respectively. In [70], the authors have classified only the first 50 sets of EEG signals of focal and non-focal classes. The features utilized to perform classification are average sample entropy (ASE) and average variance of instantaneous frequencies (AVIF) of intrinsic mode functions (IMFs) of EEG signals. They have reported a classification accuracy of 85% using the LS-SVM classifier. In [28], entropy features are extracted from the IMFs of EEG signals of focal and non-focal classes. Average Shannon, Rényi, approximate, sample and phase entropies are used for the classification of focal and non-focal EEG signals. These average entropies coupled with the LS-SVM classifier resulted in 87% classification accuracy. In these studies, features did not show any particular trend across various IMFs. However, in this study, we can clearly observe that entropy values for focal EEG signals are smaller than the non-focal EEG signals. This trend indicates that the epileptogenic brain area is less complex. Hence, the identification of focal and non-focal EEG channels can be used to characterize the epileptogenic focus.

It can be observed from Table 3 that the standard deviation of the classification performance measures is high. Hence, we developed an index to discriminate the focal and non-focal EEG classes. In this work, an integrated index and automated system are developed for the discrimination of focal and non-focal EEG signals. It can be seen from Figure 11 that these two classes are clearly separable

using a single-number FNFI. Thus, the FNFI can be helpful for epileptologists to determine the epileptogenic focus.

The proposed system has the following advantages:

- A novel discrimination index, FNFI, is proposed using three features that can identify focal and non-focal EEG signals using a single number.
- This integrated index can be used by epileptologists to cross-check their diagnosis and, hence, can reduce their workload significantly.

The limitation of the present study is the use of a small EEG database. The database used in this study contains only 50 pairs of focal EEG signals and 50 pairs of non-focal EEG signals. In order to apply the proposed method to clinical purposes, a more exhaustive study with a database containing a large number of EEG signals recorded from a number of subjects is required.

Table 5. Comparison of studies performed on the Bern-Barcelona database for automatic classification of EEG signals of focal and non-focal classes. DPE, delay permutation entropy; ASE, average sample entropy; AVIF, average variance of instantaneous frequency; IMF, intrinsic mode function.

Authors	Datasets	Features	Classifiers	Ten-fold cross-validation used	Classification accuracy (%)
Zhu *et al.* [69]	50 signals 750 signals	DPE	SVM	No	84 75
Sharma *et al.* [70]	50 signals	ASE, AVIF measures from IMFs	LS-SVM	Yes	85
Sharma *et al.* [28]	50 signals	Entropy measures from IMFs	LS-SVM	Yes	87
This work	50 signals	Entropy features from DWT	KNN, PNN, fuzzy and LS-SVM	Yes	FNFI clearly discriminates two classes

5. Conclusion

In this paper, a new method for the classification of focal EEG signals using an integrated index developed based on entropies is proposed. This technique helps to detect the unknown class of EEG signal using a single number. Furthermore, we have used entropy-based features computed from the DWT of EEG signals to perform the classification. We have also used various ranking methods for feature selection. In this work, Student's t-test- and ROC-based ranking methods are found to be most suitable. We have achieved the highest average classification accuracy of 84%, sensitivity of 84% and specificity of 84% using the LS-SVM classifier. Our study suggests that the focal EEG signals are more regular compared to non-focal EEG signals, as all entropy measures of focal EEG signals are smaller than non-focal EEG signals. By separating the EEG signals from focal and other areas of brain, the epileptogenic focus can be determined. Therefore, this novel index and proposed computer-based automatic diagnosis system can be used to identify the area of epileptogenic focus during epilepsy screening. The FNFI devised using three entropy features helps to discriminate focal and non-focal EEG signals.

In the future, the proposed methodology can be evaluated on the entire dataset. The proposed method can be studied to discriminate normal and abnormal EEG signals, like autism, Alzheimer's disease, depression, *etc*.

Author Contributions

U. Rajendra Acharya and Ram Bilas Pachori formulated the research problem. Rajeev Sharma carried out the research work. All authors contributed in writing the manuscript. All authors have read and approved the final manuscript.

Conflict of Interests

The authors declare no conflict of interest.

References

1. Cross, D.J.; Cavazos, J.E. *The Role of Sprouting and Plasticity in Epileptogenesis and Behavior*; Behavioral Aspects of Epilepsy; Demos Medical Publishing: New York, NY, USA, 2007.
2. Acharya, U.R.; Sree, S.V.; Swapna, G.; Martis, R.J.; Suri, J.S. Automated EEG analysis of epilepsy: A review. *Knowledge-Based Syst.* **2013**, *45*, 147–165.
3. Pati, S.; Alexopoulos, A.V. Pharmacoresistant epilepsy: From pathogenesis to current and emerging therapies. *Clevel. Clin. J. Med.* **2010**, *77*, 457–467.
4. Ortega, G.J.; Menendez de la Prida, L.; Sola, R.G.; Pastor, J. Synchronization clusters of interictal activity in the lateral temporal cortex of epileptic patients: Intraoperative electrocorticographic analysis. *Epilepsia* **2008**, *49*, 269–280.
5. Van Mierlo, P.; Carrette, E.; Hallez, H.; Raedt, R.; Meurs, A.; Vandenberghe, S.; Van Roost, D.; Boon, P.; Staelens, S.; Vonck, K. Ictal-onset localization through connectivity analysis of intracranial EEG signals in patients with refractory epilepsy. *Epilepsia* **2013**, *54*, 1409–1418.
6. Towle, V.L.; Carder, R.K.; Khorasani, L.; Lindberg, D. Electrocorticographic coherence patterns. *J. Clin. Neurophysiol.* **1999**, *16*, 528–547.
7. Schevon, C.A.; Cappell, J.; Emerson, R.; Isler, J.; Grieve, P.; Goodman, R.; Mckhann, G., Jr.; Weiner, H.; Doyle, W.; Kuzniecky, R.; Devinsky, O.; Gilliam, F. Cortical abnormalities in epilepsy revealed by local EEG synchrony. *NeuroImage* **2007**, *35*, 140–148.
8. Lehnertz, K.; Elger, C. Spatio-temporal dynamics of the primary epileptogenic area in temporal lobe epilepsy characterized by neuronal complexity loss. *Electroencephalogr. Clin. Neurophysiol.* **1995**, *95*, 108–117.
9. Andrzejak, R.G.; Schindler, K.; Rummel, C. Nonrandomness, nonlinear dependence, and nonstationarity of electroencephalographic recordings from epilepsy patients. *Phys. Rev. E* **2012**, *86*, 046206.
10. Gajic, D.; Djurovic, Z.; Gligorijevic, J.; Di Gennaro, S.; Savic-Gajic, I. Detection of epileptiform activity in EEG signals based on time-frequency and nonlinear analysis. *Front. Comput. Neurosci.* **2015**, *9*.

11. Gajic, D.; Djurovic, Z.; Di Gennaro, S.; Gustafsson, F. Classification of EEG signals for detection of epileptic seizures based on wavelets and statistical pattern recognition. *Biomed. Eng. Appl. Basis Commun.* **2014**, *26*, 1450021.
12. Subasi, A. EEG signal classification using wavelet feature extraction and a mixture of expert model. *Expert Syst. Appl.* **2007**, *32*, 1084–1093.
13. Kannathal, N.; Choo, M.L.; Acharya, U.R.; Sadasivan, P.K. Entropies for detection of epilepsy in EEG. *Comput. Methods Progr. Biomed.* **2005**, *80*, 187–194.
14. Acharya, U.R.; Molinari, F.; Sree, S.V.; Chattopadhyay, S.; Ng, K.H.; Suri, J.S. Automated diagnosis of epileptic EEG using entropies. *Biomed. Signal Process. Control* **2012**, *7*, 401–408.
15. Daubechies, I. *Ten Lectures on Wavelets*; SIAM: Philadelphia, PA, USA, 1992.
16. Acharya, U.R.; Vidya, K.S.; Ghista, D.N.; Lim, W.J.E.; Molinari, F.; Sankaranarayanan, M. Computer-aided diagnosis of diabetic subjects by heart rate variability signals using discrete wavelet transform method. *Knowledge-Based Syst.* **2015**, *81*, 56–64.
17. Rosso, O.A.; Blanco, S.; Yordanova, J.; Kolev, V.; Figliola, A.; Schürmann, M.; Başar, E. Wavelet entropy: A new tool for analysis of short duration brain electrical signals. *J. Neurosci. Methods* **2001**, *105*, 65–75.
18. Rényi, A. On measures of entropy and information. In *Proceedings of the Fourth Berkeley Symposium on Mathematical Statistics and Probability: Contributions to the Theory of Statistics*; University of California Press: Berkeley, CA, USA, 1961; Volume 1, pp. 547–561.
19. Chen, J.; Li, G. Tsallis wavelet entropy and its application in power signal analysis. *Entropy* **2014**, *16*, 3009–3025.
20. Ramirez-Villegas, J.F.; Ramirez-Moreno, D.F. Wavelet packet energy, Tsallis entropy and statistical parameterization for support vector-based and neural-based classification of mammographic regions. *Neurocomputing* **2012**, *77*, 82–100.
21. Chen, W.; Wang, Z.; Xie, H.; Yu, W. Characterization of surface EMG signal based on fuzzy entropy. *IEEE Trans. Neural Syst. Rehabil. Eng.* **2007**, *15*, 266–272.
22. Xie, H.B.; Chen, W.T.; He, W.X.; Liu, H. Complexity analysis of the biomedical signal using fuzzy entropy measurement. *Appl. Soft Comput.* **2011**, *11*, 2871–2879.
23. Nicolaou, N.; Georgiou, J. Detection of epileptic electroencephalogram based on permutation entropy and support vector machine. *Expert Syst. Appl.* **2012**, *39*, 202–209.
24. Bandt, C.; Pompe, B. Permutation entropy: A natural complexity measure for time series. *Phys. Rev. Lett.* **2002**, *88*, 174102.
25. Riedl, M.; Müller, A.; Wessel, N. Practical considerations of permutation entropy. *Eur. Phys. J. Spec. Top.* **2013**, *222*, 249–262.
26. Acharya, U.R.; Sree, S.V.; Ang, P.C.A.; Yanti, R.; Suri, J.S. Application of non-linear and wavelet based features for the automated identification of epileptic EEG signals. *Int. J. Neural Syst.* **2012**, *22*, 1250002.
27. Chua, K.C.; Chandran, V.; Acharya, U.R.; Lim, C.M. Analysis of epileptic EEG signals using higher order spectra. *J. Med. Eng. Technol.* **2009**, *33*, 42–50.

28. Sharma, R.; Pachori, R.B.; Acharya, U.R. Application of entropy measures on intrinsic mode functions for the automated identification of focal electroencephalogram signals. *Entropy* **2015**, *17*, 669–691.
29. Acharya, U.R.; Ng, E.Y.K.; Eugene, L.W.J.; Noronha, K.P.; Min, L.C.; Nayak, K.P.; Bhandary, S.V. Decision support system for the glaucoma using Gabor transformation. *Biomed. Signal Process. Control* **2015**, *15*, 18–26.
30. Kailath, T. The divergence and Bhattacharyya distance measures in signal selection. *IEEE Trans. Commun. Technol.* **1967**, *15*, 52–60.
31. Zhu, W.; Wang, X.; Ma, Y.; Rao, M.; Glimm, J.; Kovach, J.S. Detection of cancer-specific markers amid massive mass spectral data. *Proc. Natl. Acad. Sci. USA* **2003**, *100*, 14666–14671.
32. Derryberry, D.R.; Schou, S.B.; Conover, W.J. Teaching rank-based tests by emphasizing structural similarities to corresponding parametric tests. *J. Stat. Educ.* **2010**, *18*, 1–19.
33. Kruskal, W.H. Historical notes on the Wilcoxon unpaired two-sample test. *J. Am. Stat. Assoc.* **1957**, *52*, 356–360.
34. Mann, H.B.; Whitney, D.R. On a test of whether one of two random variables is stochastically larger than the other. *Ann. Math. Stat.* **1947**, *18*, 50–60.
35. Bergmann, R.; Ludbrook, J.; Spooren, W.P.J.M. Different outcomes of the Wilcoxon-Mann-Whitney test from different statistics packages. *Am. Stat.* **2000**, *54*, 72–77.
36. Theodoridis, S.; Koutroumbas, K. Feature selection. In *Pattern Recognition*, second ed.; Academic Press: San Diego, CA, USA, 2003; pp. 163–205.
37. Kohavi, R. A study of cross-validation and bootstrap for accuracy estimation and model selection. In Proceedings of the 14th International Joint Conference on Artificial Intelligence (IJCAI-95), Montreal, QC, Canada, 20–25 August 1995; Morgan Kaufmann: San Francisco, CA, USA, 1995; pp. 1137–1143.
38. Swapna, G.; Acharya, U.R.; Sree, S.V.; Suri, J.S. Automated detection of diabetes using higher order spectral features extracted from heart rate signals. *Intell. Data Anal.* **2013**, *17*, 309–326.
39. Mao, K.; Tan, K.C.; Ser, W. Probabilistic neural-network structure determination for pattern classification. *IEEE Trans. Neural Netw.* **2000**, *11*, 1009–1016.
40. Han, J.; Kamber, M.; Pei, J. Classification: Advanced methods. In *Data Mining*, 3rd ed.; Kamber, J.H., Pei, J., Eds.; The Morgan Kaufmann Series in Data Management Systems; Morgan Kaufmann: Boston, MA, USA, 2012; pp. 393–442.
41. Ishibuchi, H.; Nakashima, T. Improving the performance of fuzzy classifier systems for pattern classification problems with continuous attributes. *IEEE Trans. Ind. Electron.* **1999**, *46*, 1057–1068.
42. Acharya, U.R.; Sree, S.V.; Chattopadhyay, S.; Yu, W.; Ang, P.C.A. Application of recurrence quantification analysis for the automated identification of epileptic EEG signals. *Int. J. Neural Syst.* **2011**, *21*, 199–211.
43. Acharya, U.R.; Sree, S.V.; Ang, P.C.A.; Yanti, R.; Suri, J.S. Application of non-linear and wavelet based features for the automated identification of epileptic EEG signals. *Int. J. Neural Syst.* **2012**, *22*, 1250002.
44. Vapnik, V.N. *The Nature of Statistical Learning Theory*; Springer: New York, NY, USA, 2000.

45. Suykens, J.A.K.; Vandewalle, J. Least squares support vector machine classifiers. *Neural Process. Lett.* **1999**, *9*, 293–300.
46. Pachori, R.B.; Sharma, R.; Patidar, S. Classification of normal and epileptic seizure EEG signals based on empirical mode decomposition. In *Complex System Modelling and Control Through Intelligent Soft Computations*; Zhu, Q., Azar, A.T., Eds.; Springer: Switzerland, 2015; Volume 319, pp. 367–388.
47. Joshi, V.; Pachori, R.B.; Vijesh, A. Classification of ictal and seizure-free EEG signals using fractional linear prediction. *Biomed. Signal Process. Control* **2014**, *9*, 1–5.
48. Sharma, R.; Pachori, R.B. Classification of epileptic seizures in EEG signals based on phase space representation of intrinsic mode functions. *Expert Syst. Appl.* **2015**, *42*, 1106–1117.
49. Ghista, D.N. Physiological systems' numbers in medical diagnosis and hospital cost-effective operation. *J. Mech. Med. Biol.* **2004**, *4*, 401–418.
50. Acharya, U.R.; Faust, O.; Sree, S.V.; Ghista, D.N.; Dua, S.; Joseph, P.; Ahamed, V.I.T.; Janarthanan, N.; Tamura, T. An integrated diabetic index using heart rate variability signal features for diagnosis of diabetes. *Comput. Methods Biomech. Biomed. Eng.* **2011**, *16*, 222–234.
51. Acharya, U.R.; Sree, S.V.; Krishnan, M.M.R.; Krishnananda, N.; Ranjan, S.; Umesh, P.; Suri, J.S. Automated classification of patients with coronary artery disease using grayscale features from left ventricle echocardiographic images. *Comput. Methods Programs Biomed.* **2013**, *112*, 624–632.
52. Acharya, U.R.; Faust, O.; Sree, S.V.; Molinari, F.; Garberoglio, R.; Suri, J.S. Cost-effective and non-invasive automated benign & malignant thyroid lesion classification in 3D contrast-enhanced ultrasound using combination of wavelets and textures: A class of ThyroScan^{TM} algorithms. *Technol. Cancer Res. Treat.* **2011**, *10*, 371–380.
53. Patidar, S.; Pachori, R.B.; Acharya, U.R. Automated diagnosis of coronary artery disease using tunable-Q wavelet transform applied on heart rate signals. *Knowledge-Based Syst.* **2015**, *82*, 1–10.
54. Acharya, U.R.; Ng, E.Y.K.; Tan, J.H.; Sree, S.V.; Ng, K.H. An integrated index for the identification of diabetic retinopathy stages using texture parameters. *J. Med. Syst.* **2012**, *36*, 2011–2020.
55. Ocak, H. Optimal classification of epileptic seizures in EEG using wavelet analysis and genetic algorithm. *Signal Process.* **2008**, *88*, 1858–1867.
56. Yuen, S.Y.; Chow, C.K. A genetic algorithm that adaptively mutates and never revisits. *IEEE Trans. Evol. Comput.* **2009**, *13*, 454–472.
57. McKight, P.E.; Najab, J. Kruskal-Wallis Test. *Corsini Encycl. Psychol.* **2010**.
58. Pachori, R.B. Discrimination between ictal and seizure-free EEG signals using empirical mode decomposition. *Res. Lett. Signal Process.* **2008**, *2008*, 293056.
59. Pachori, R.B.; Bajaj, V. Analysis of normal and epileptic seizure EEG signals using empirical mode decomposition. *Comput. Methods Programs Biomed.* **2011**, *104*, 373–381.
60. Shah, M.; Saurav, S.; Sharma, R.; Pachori, R.B. Analysis of epileptic seizure EEG signals using reconstructed phase space of intrinsic mode functions. In Proceedings of 9th International Conference on Industrial and Information Systems, Gwalior, India, 15–17 December 2014; pp. 1–6.

61. Pachori, R.B.; Avinash, P.; Shashank, K.; Sharma, R.; Acharya, U.R. Application of empirical mode decomposition for analysis of normal and diabetic RR-interval signals. *Expert Syst. Appl.* **2015**, *42*, 4567–4581.
62. Azar, A.T.; El-Said, S.A. Performance analysis of support vector machines classifiers in breast cancer mammography recognition. *Neural Comput. Appl.* **2014**, *24*, 1163–1177.
63. Naro, D.; Rummel, C.; Schindler, K.; Andrzejak, R.G. Detecting determinism with improved sensitivity in time series: Rank-based nonlinear predictability score. *Phys. Rev. E* **2014**, *90*, 032913.
64. Subramaniyam, N.P.; Hyttinen, J. Dynamics of intracranial electroencephalographic recordings from epilepsy patients using univariate and bivariate recurrence networks. *Phys. Rev. E* **2015**, *91*, 022927.
65. Ben-Jacob, E.; Doron, I.; Gazit, T.; Rephaeli, E.; Sagher, O.; Towle, V.L. Mapping and assessment of epileptogenic foci using frequency-entropy templates. *Phys. Rev. E* **2007**, *76*, 051903.
66. Marciani, M.G.; Stefanini, F.; Stefani, N.; Maschio, M.C.E.; Gigli, G.L.; Roncacci, S.; Caltagirone, C.; Bernardi, G. Lateralization of the epileptogenic focus by computerized EEG study and neuropsychological evaluation. *Int. J. Neurosci.* **1992**, *66*, 53–60.
67. Sabesan, S.; Good, L.B.; Tsakalis, K.S.; Spanias, A.; Treiman, D.M.; Iasemidis, L.D. Information flow and application to epileptogenic focus localization from intracranial EEG. *IEEE Trans. Neural Syst. Rehabil. Eng.* **2009**, *17*, 244–253.
68. Warren, C.P.; Hu, S.; Stead, M.; Brinkmann, B.H.; Bower, M.R.; Worrell, G.A. Synchrony in normal and focal epileptic brain: The seizure onset zone is functionally disconnected. *J. Neurophysiol.* **2010**, *104*, 3530–3539.
69. Zhu, G.; Li, Y.; Wen, P.P.; Wang, S.; Xi, M. Epileptogenic focus detection in intracranial EEG based on delay permutation entropy. In Proceeding of 2013 International Symposium on Computational Models for Life Science, Sydney, Australia, 27–29 November 2013; Volume 1559; pp. 31–36.
70. Sharma, R.; Pachori, R.B.; Gautam, S. Empirical mode decomposition based classification of focal and non-focal EEG signals. In Proceedings of 2014 International Conference on Medical Biometrics, Shenzhen, China, 30 May–1 June 2014; pp. 135–140.